

PAPER

Scattering lifetime and high figure of merit in CsAgO predicted by methods beyond relaxation time approximation

To cite this article: Vineet Kumar Sharma *et al* 2022 *J. Phys.: Condens. Matter* **34** 295502

View the [article online](#) for updates and enhancements.

You may also like

- [Odyssey of thermoelectric materials: foundation of the complex structure](#)
Khalid Bin Masood, Pushpendra Kumar, R A Singh et al.
- [Review of the thermoelectric properties of layered oxides and chalcogenides](#)
A I Romanenko, G E Chebanova, Tingting Chen et al.
- [Physics and technology of thermoelectric materials and devices](#)
Akshara Dadhich, Madhuvathani Saminathan, Kaushalya Kumari et al.

Scattering lifetime and high figure of merit in CsAgO predicted by methods beyond relaxation time approximation

Vineet Kumar Sharma¹, V Kanchana^{1,*} , Mayanak K Gupta^{2,3}  and Ranjan Mittal^{2,3} 

¹ Department of Physics, Indian Institute of Technology Hyderabad, Kandi 502285, Sangareddy, Telangana, India

² Solid State Physics Division, Bhabha Atomic Research Centre Trombay, Mumbai 400085, India

³ Homi Bhabha National Institute, Anushaktinagar, Mumbai 400094, India

E-mail: kanchana@iith.ac.in

Received 3 February 2022, revised 28 April 2022

Accepted for publication 9 May 2022

Published 25 May 2022



Abstract

The electronic transport behaviour of CsAgO has been discussed using the theory beyond relaxation time approximation from room temperature to 800 K. Different scattering mechanisms such as acoustic deformation potential scattering, impurity phonon scattering, and polar optical phonon scattering are considered for calculating carrier scattering rates to predict the absolute values of thermoelectric coefficients. The scattering lifetime is of the order of 10^{-14} s. The lattice thermal transport properties like lattice thermal conductivity and phonon-lifetime have been evaluated. The calculated lattice thermal conductivity equals 0.12 and 0.18 W mK⁻¹ along 'a' and 'c' axes, respectively, at room temperature, which is very low compared to state-of-the-art thermoelectric materials. The anisotropy in the electrical conductivity indicates that the holes are favourable for the out-of-plane thermoelectrics while the electrons for in-plane thermoelectrics. The thermoelectric figure of merit for holes and electrons is nearly same with a value higher than 1 at 800 K for different doping concentrations. The value of the thermoelectric figure of merit is significantly higher than the existing oxide materials, which might be appealing for future applications in CsAgO.

Keywords: thermal conductivity, carrier lifetime, thermoelectric figure of merit

(Some figures may appear in colour only in the online journal)

1. Introduction

The reduction in fossil fuels led to the invention of highly efficient renewable energy harvesting sources in addition to the existing ones. Thermoelectricity could be considered as one such resources which converts waste heat into electricity. Because of this feature, it has attracted the modern era of scientists to uncover productive resources. A lot of research has been done in this field, especially on chalcogenides like

Bi₂Se₃ and Sb₂Te₃, which still need to be explored. Real device applications demand the best materials with promising outputs, which motivates us to explore various materials. A wide range of materials like thin-film superlattice, large single-crystal or polycrystalline bulk materials, semiconductors and semimetals, and many more have been chosen with an objective to enhance their efficiency or to find an alternative choice [1–4]. The thermoelectric materials have various commercial applications, covering a wide range from electronic refrigeration and power generation to power heart pacemakers. The radioisotope thermoelectric generators are being used

* Author to whom any correspondence should be addressed.

as a power source in space. The recent invention revealed that thermoelectric materials were used in the new generation of vehicles to transform waste heat into electricity provided for automotive electrical systems and thereby increase fuel efficiency [5].

Although, a plethora of research has been done to explore better thermoelectric materials and examine their performance, only very few materials fetch commercial applications, which include chalcogenides [6–8], and pnictides [9–14]. The modern era of research urges those materials which are thermodynamically stable, anti-oxidant, cost-effective, environment-friendly and possess high operating temperatures. To date, the well-known commercial TE devices are made up of either pnictogens or chalcogens, which are toxic or scarce in nature, and lacks high temperature applications together with a tendency to get oxidized in air [15–17]. These properties of traditional thermoelectrics pushed researchers ahead to look for alternative materials and found that the metal oxides could be a suitable candidate for TE applications as they host all the features lacking in traditional TE materials [18]. Among oxide materials, copper oxides were explored by various group [19–21] for their high thermopower. The recent studies on p-type Na_xCoO_2 , SrTiO_3 , and other layered Co-based materials brought up a revolution which led to a new generation of TE materials [18]. These materials can operate at high temperatures, but their high thermal conductivity is a major challenge that reduces the efficiency.

The limitations observed in previously found oxide materials pose a challenge for the scientists and researchers to find materials with low thermal transport and high electron conduction to improve their efficiency. These previous studies and challenges related to promising device applications encourage us to explore new metallic oxide in conjunction with alkali atom, CsAgO. Except experimental synthesis and crystal structure details [22, 23], there are no other studies available on this compound. A theoretical study on similar class of oxide materials by Umamaheshwari *et al* [24] reported the structural phase transition and their electronic properties, which revealed that out of two tetragonal phases: $I4m2(119)$ and $I4/mmm(139)$, later one is more stable, and we have considered the same in our calculations. The present work discusses the electronic structure properties and their correlation to transport properties. The major highlight of this work is to discuss the transport properties using the methods beyond relaxation time approximation and high-temperature figure of merit. This paper is organized as follows, section 2 discusses all the computational methods used, followed by section 3 where the lattice dynamics, electronic, and transport properties are discussed. Finally, section 3.4 summarizes the work.

2. Computational methods and crystal structure

The projector augmented wave method implemented in Vienna *ab initio* Simulation Package (VASP) [25–27] was used to carry out the first-principles calculations. We have used three different exchange–correlation functionals like GGA-PBE

[28], LDA [29] and PBEsol [30] to get the ground state parameters close to the experimental one. We found that the lattice parameters with PBEsol functional are in better agreement with experiment parameters ($a = 10.24 \text{ \AA}$, $c = 6.17 \text{ \AA}$) taken for our calculations. The energy cut off for plane-wave basis is taken to be 900 eV along with the energy and force tolerance 10^{-8} eV and 10^{-2} eV \AA^{-1} . A $4 \times 4 \times 8$ Γ -centered k -mesh is used for Brillouin zone sampling using the tetrahedron method [31]. The frozen phonon method has been used to calculate the force constants using the VASP package, which was further used to plot phonon spectra through Phonopy [32]. Higher-order displacement files are generated with a finite displacement of around 0.03 \AA using the supercell method, which is used further to compute the lattice thermal conductivity (κ_l) using both phono3py [33] and VASP through second and third-order force constants. The carrier scattering lifetime and transport properties are calculated using AMSET code [34], where different scattering mechanisms are taken into account to predict the TE coefficients. CsAgO belongs to body-centered tetragonal structure with space group $I4/mmm$ (No. 139), and the same is shown in figure 1(b).

3. Results and discussion

3.1. Phonon dispersion and lattice thermal conductivity

We present the calculated phonon spectrum of CsAgO in figure 2(a). We observe a frequency gap between mid- and high-frequency optical modes contributed by different elements differing in their atomic masses. The heavier elements correspond to low-frequency phonon modes, whereas the lighter one corresponds to higher frequency phonon modes. Most of the phonon branches dominate low-frequency regions, which drive the anharmonicity in the system together with enhanced scattering. The anharmonic nature can be understood from the softening of one of the acoustic modes, and hints at the possible low lattice thermal transport in the investigated compound. Next, we have calculated the temperature-dependent lattice thermal conductivity (κ_l) using the harmonic and anharmonic interatomic force constants along ‘ a ’ and ‘ c ’ axes. We observe that κ_l decreases as a function of temperature and remains anisotropic throughout the studied temperature range. The value of κ_l around 300 K is 0.12, and 0.18 W mK^{-1} along ‘ a ’ and ‘ c ’ axes, respectively. These values are appreciably smaller than the well-known thermoelectric materials [35]. To substantiate further on the low lattice thermal conductivity, we have predicted the Grüneisen parameter through elastic moduli and plotted the frequency-dependent phonon lifetime from third-order force constants. The value of Grüneisen parameter is 1.73, which is high and in line with other well-known thermoelectrics [35]. The calculated phonon lifetime is given in figure 2(c). The color bar represents the density of phonon modes, and black dots are phonon modes. Red and blue colors indicate maximum and minimum values of phonon density. The lifetime of phonon modes corresponding to low-frequency phonon modes is very short due to highly interacting phonon modes. We claim that the anharmonicity observed in

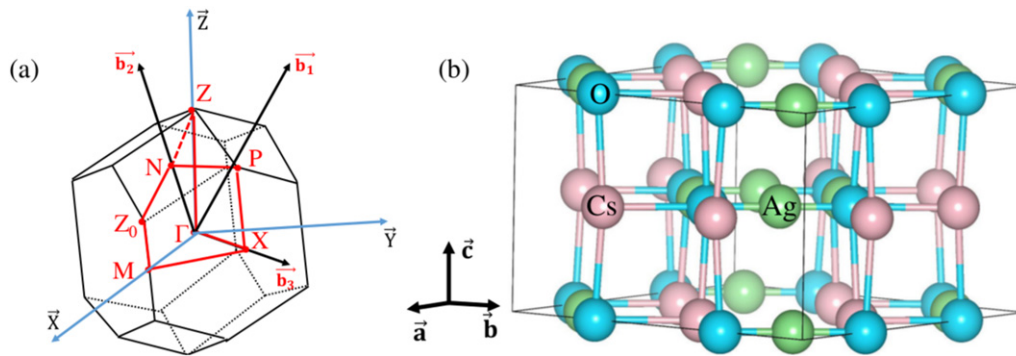


Figure 1. (a) The irreducible Brillouin zone and (b) crystal structure of CsAgO, pink, green and blue colors represents Cs, Ag and O atoms, respectively.

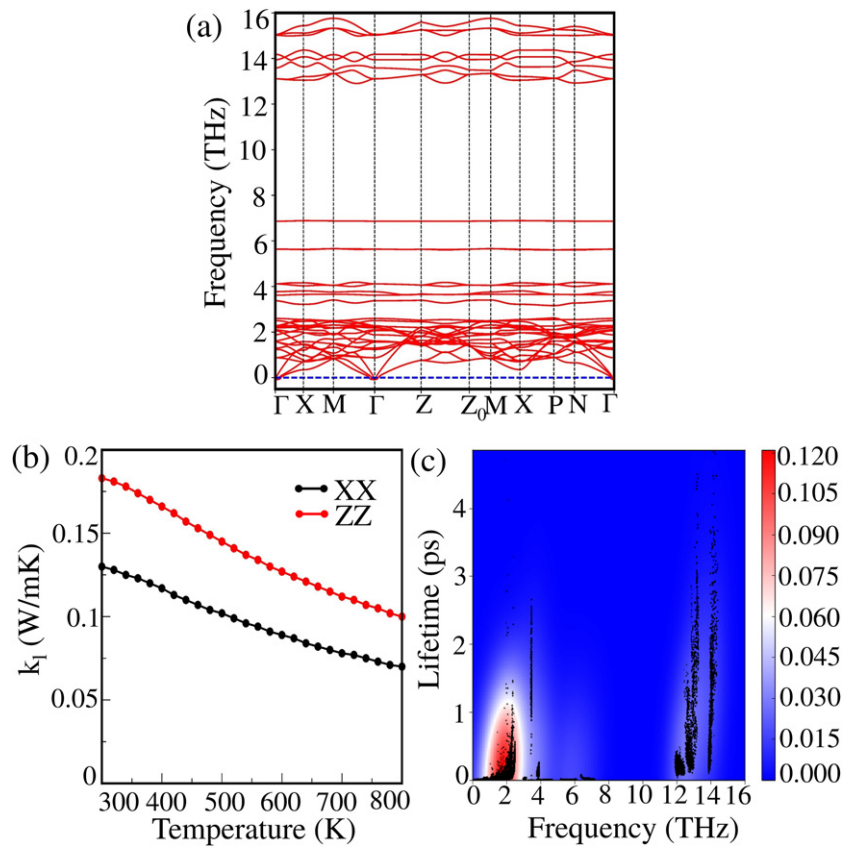


Figure 2. (a) The phonon band dispersion illustrating the highly interacting low-frequency phonon modes and anharmonic nature at zone centre Γ , (b) lattice thermal conductivity is presented along ‘a’ and ‘c’ axes, and (c) phonon-lifetime as a function of frequency, the color bar indicates the density of phonon modes. Red and blue colors correspond to maximum and minimum density.

phonon modes mainly causes the low lattice thermal transport. The lifetime values and high Grüneisen parameter are the evidence for it.

3.2. Electronic band structure and scattering lifetime

The calculated electronic structure properties for CsAgO are given in figure 3. The band structure plot shows a direct bandgap semiconducting nature with a bandgap of 1.44 eV. There are no previous experimental or theoretical reports available on electronic structure properties for CsAgO which limits us to do a comparison. The band dispersion in both the

conduction and valence band regions around the Fermi level is significantly different, especially along both the crystallographic axes. The bands lying near the Fermi level are dominated by O-*p* and Ag-*d* orbitals with negligible contribution of Ag atom as confirmed from the total density of states and partial density of states plot [figure 3(b)]. The dispersive and flat nature of bands near the Fermi level are incremental for thermoelectric properties here, and the same are discussed in the upcoming section. Before starting the discussion on thermoelectric properties, one need to calculate the carrier scattering lifetime, which is necessary to predict the absolute value of

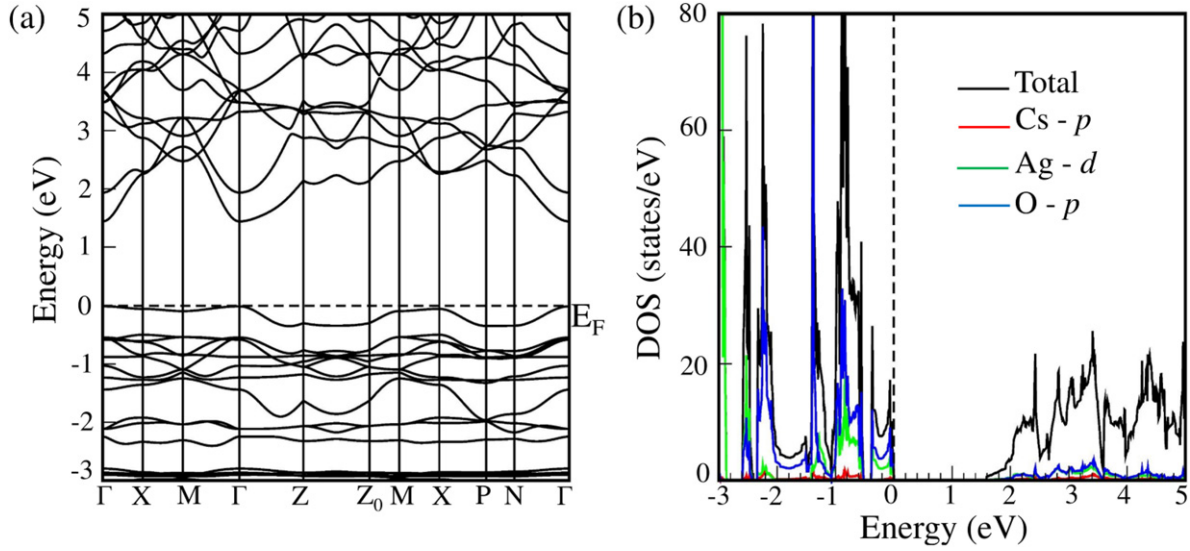


Figure 3. (a) The electronic band structure plotted along high-symmetry points as shown in Brillouin zone figure 1(a). (b) The total and orbital projected density of states.

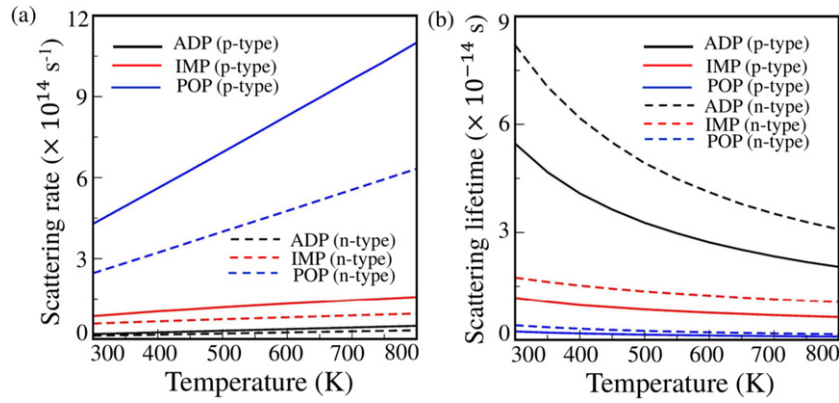


Figure 4. The temperature dependent scattering rates in (a) and the scattering lifetime in (b) respectively. p-type corresponds to holes and n-type for electrons. The scattering lifetime for electrons is shorter than that of holes.

transport properties like the electrical conductivity or mobility. We have considered several scattering factors responsible for either acoustic phonon–electron or optical phonon–electron interactions as implemented in the software package AMSET [34]. These factors are deformation potential, impurities and displacement of atoms. The deformation potential is responsible for acoustic phonon–electron interaction leading to low-temperature effects known as acoustic deformation potential scattering. Every system always hosts impurities that scatter electrons and known as impurity scattering. The third one is the polar optical phonon scattering (POP) driven by the displacement of atoms and contributed by optical phonon modes, which dominate in high-temperature regimes. The scattering may be elastic or inelastic. The elastic scattering is state-independent and contributed by acoustic phonon branches. In contrast, inelastic scattering is state dependent and fully dominated by optical phonon branches. Depending upon the differences in both types of scatterings, we have used two different approximations: the momentum relaxation time approximation for the elastic scattering and self-energy relaxation time

approximation for inelastic scattering one. The scattering rate for elastic scattering case from state nk to $mk + q$ is calculated using Fermi’s golden rule and can be given by,

$$\tau_{nk \rightarrow mk+q}^{-1} = \frac{2\pi}{\hbar} |g_{nm}(k, q)|^2 \times \delta(\Delta\epsilon_{k,q}^{nm}). \quad (1)$$

A similar type of expression has been used to calculate the scattering rate for the inelastic scattering case for the state from nk to $mk + q$, which is given as,

$$\begin{aligned} \tau_{nk \rightarrow mk+q}^{-1} = & \frac{2\pi}{\hbar} |g_{nm}(k, q)|^2 \\ & \times \delta[(n_q + 1 - f_{mk+q}^0)\delta(\Delta\epsilon_{k,q}^{nm} - \hbar\omega_q) \\ & + (n_q + f_{mk+q}^0)\delta(\Delta\epsilon_{k,q}^{nm} + \hbar\omega_q)], \end{aligned} \quad (2)$$

where $-\hbar\omega_q$ and $\hbar\omega_q$ correspond to a phonon’s emission and absorption, respectively. The scattering rate and scattering lifetime as a function of temperature for fixed doping concentration around 10^{19} cm^{-3} are given in figure 4. The POP dominates, as seen from the plots, reflecting the role of optical

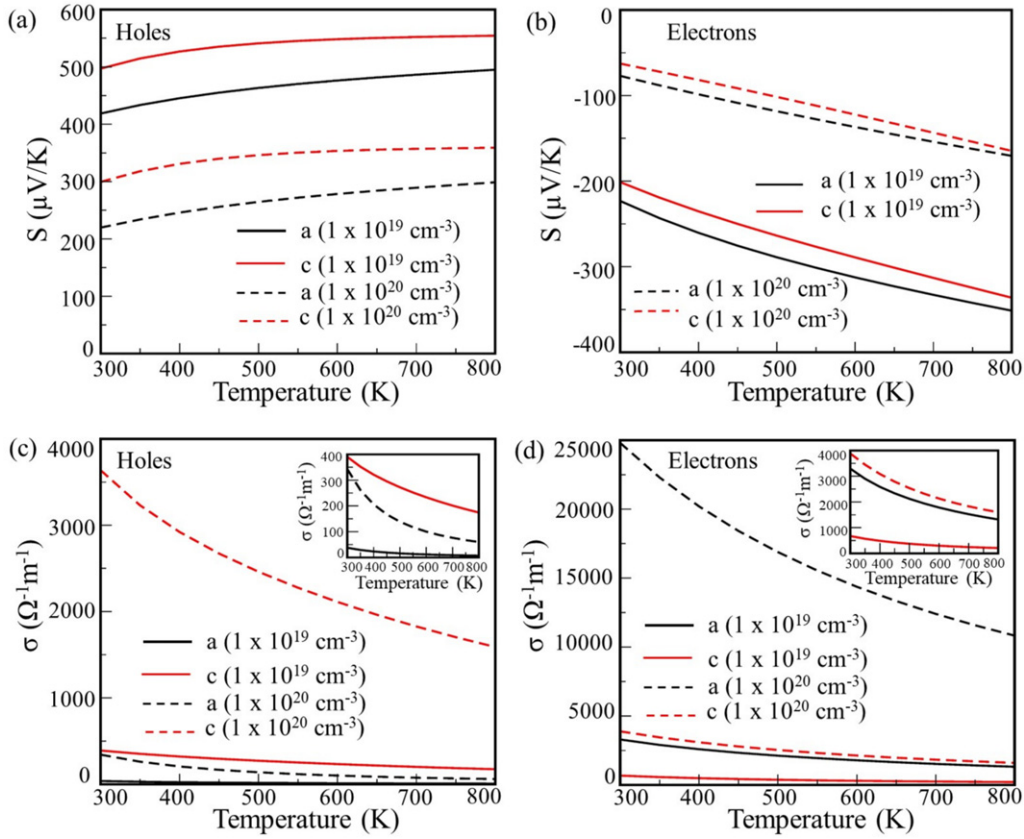


Figure 5. The carrier concentration and temperature dependent thermopower is given in top panel (a) and (b). The bottom panel (c) and (d) shows the electrical conductivity (c) and (d) for both the holes and electrons respectively.

phonons in high-temperature ranges. The calculated scattering lifetime values are of the order of 10^{-14} s [figure 4(b)], which is further used to estimate the absolute value of TE coefficients. In addition, we have calculated scattering rate and scattering lifetime at carrier concentration around 10^{20} cm⁻³, and observed the nearly similar values of carrier lifetime noted at carrier concentration around 10^{19} cm⁻³ [not shown for brevity].

3.3. Thermoelectric properties

The low lattice thermal transport and highly dispersive electronic bandstructure further prompt us to explore the thermoelectric properties for wide temperature ranges. The temperature and carrier-dependent thermopower is given in figures 5(a) and (b) for hole and electrons, respectively. The magnitude of thermopower increases with temperature, a genuine trend observed in all semiconductors. Thermopower for holes is higher by nearly $100 \mu\text{V K}^{-1}$ in magnitude than the value for electrons for temperature ranging from 300–800 K and displays more anisotropy [figures 5(a) and (b)]. This anisotropic behavior is due to variations of band dispersion near the Fermi level along both ‘a’ and ‘c’ axes. The band profile in the conduction band region is similar along both ‘a’ and ‘c’ axes, reflecting on isotropic ‘S’ values of electrons. On the other hand, the bands are nearly flat along the ‘a’ axis and dispersive along the ‘c’ axis in the valence band region, resulting in the anisotropic nature and higher thermopower

for holes. To observe the effect of carrier concentration, we have plotted thermopower for carrier concentrations around 10^{19} cm⁻³ and 10^{20} cm⁻³. The thermopower values are significantly dropping at higher concentrations. The calculated electrical conductivity is presented in figures 5(c) and (d). The value of electrical conductivity for holes is a few hundred at carrier concentration 10^{19} cm⁻³ which is improved by one order in magnitude for concentration around 10^{20} cm⁻³, especially along the ‘c’ axis. In the case of electrons, the scenario is quite similar, and the electrical conductivity values are 10 times higher than those for holes due to a more dispersive band profile in the conduction band. The anisotropy is more pronounced in the electrical conductivity than observed in thermopower plots, as shown in insets.

Now, we would like to discuss another important TE property called power factor and shown in figures 6(a) and (b). We can visualize the anisotropic nature similar to that observed in the other two TE properties. The power factor is decreasing with temperature as the electrical conductivity does. From the plots, we can conclude that the effect of electrical conductivity is reflected more than that of thermopower. The values of power factor for holes are lying of the order of 10^{-5} W mK⁻², whereas the electron power factor is in the order of 10^{-4} W mK⁻². Furthermore, we have computed the figure of merit of this compound to predict the thermoelectric efficiency [figures 6(c) and (d)]. The figure of merit at 800 K for holes for carrier concentration 10^{19} cm⁻³ is around 0.03,

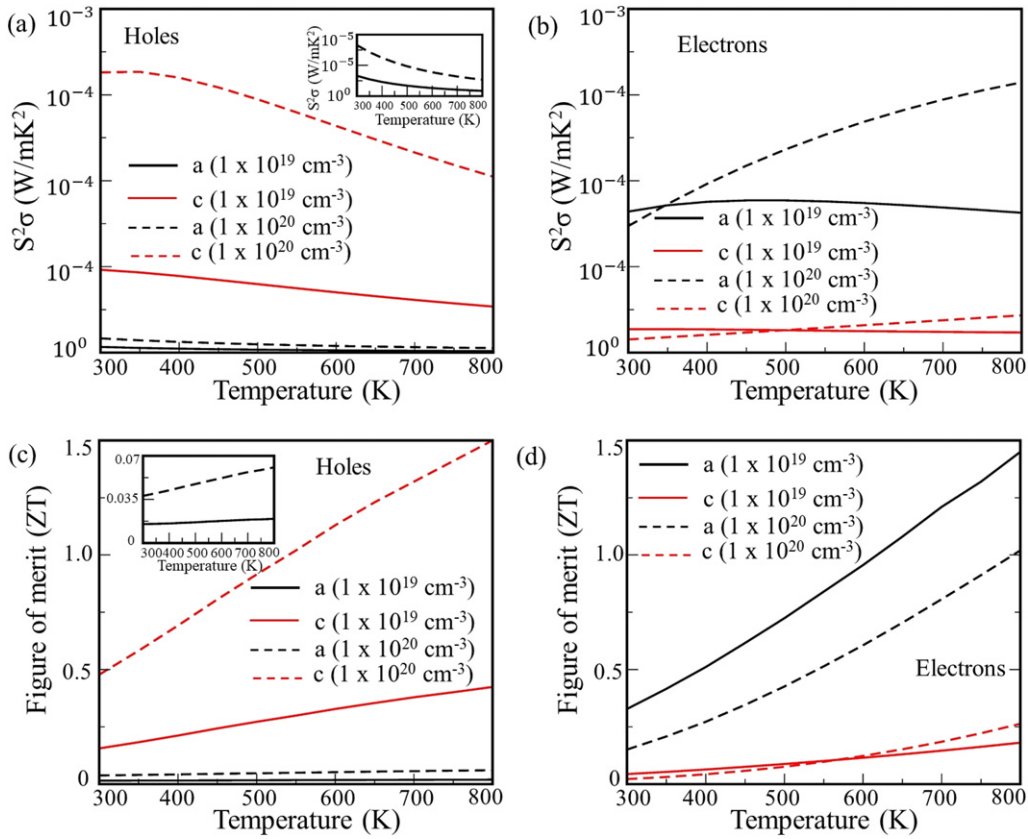


Figure 6. The carrier concentration and temperature dependent power factor in top panel (a) and (b). The bottom panel (c) and (d) shows the figure of merit (b) for both the holes and electrons respectively.

Table 1. Comparative analysis of thermoelectric figure of merit in CsAgO with other known oxide thermoelectric materials.

Compound	ZT (300 K)	ZT (800 K)
BiCuTeO [36]	0.3	0.72
Na _x CoO _{2-δ} [37]	0.03	1.2
SnO [38]	0.01	—
Co _{2.75} Gd _{0.25} Co ₄ O ₉ [18]	0.07	—
CsAgO (present work)	0.3	1.44

which is enhanced up to 1.5 along ‘c’ direction for higher concentrations. The figure of merit for electrons at 800 K is 1.2 along the ‘a’ axis for optimal doping value of 10^{19} cm^{-3} itself. The figure of merit for electrons decreases with heavy doping concentration. The calculated figure of merit is found to be higher than other known oxide materials and comparative analysis is given in table 1 [18, 36–38]. Overall, we can summarize that the calculated thermoelectric properties are highly anisotropic, suitable for low-dimension device applications. The electrons are favorable for in-plane TE application at optimal doping concentration, whereas holes could be considered for out-of-plane TE applications with heavy doping cases.

3.4. Conclusion

In summary, the theoretical modeling of lattice dynamics, carrier lifetime, electronic structure properties, and thermoelectric properties beyond the relaxation time approximation of CsAgO is presented herein. The anharmonic acoustic phonons observed in the phonon spectrum signals more scattering in the system, resulting in low lattice thermal conductivity. The calculated lattice thermal conductivity is 0.12 and 0.18 W mK^{-1} along ‘a’ and ‘c’ axes, respectively, at 300 K. The high value of Grüneisen parameter together with shorter phonon-lifetime further substantiate it. The electronic bandgap is 1.44 eV , which agrees with previous theoretical values. We have calculated temperature-dependent scattering lifetime, including different scattering schemes to get the absolute value of transport properties. The scattering lifetime is found to be around 10^{-14} s . The calculated thermoelectric properties are anisotropic, as noted from the thermopower and electrical conductivity values. Another TE parameter, the power factor, is dominated by the electrical conductivity, and the calculated figure of merit for electrons at 800 K is more than 1 at the optimal concentration value for semiconductors. The calculated figure of merit is better than the values of other well-known oxide materials, enabling future thermoelectric applications and awaits experimental verification.

Acknowledgment

Both VKS and VK would like to acknowledge IIT Hyderabad for providing computational facilities. VKS would like to acknowledge MoE for fellowship. The authors would like to acknowledge BRNS project with sanction No. (58/14/13/2019-BRNS).

Data availability statement

The data that support the findings of this study are available upon reasonable request from the authors.

ORCID iDs

V Kanchana  <https://orcid.org/0000-0003-1575-9936>
 Mayanak K Gupta  <https://orcid.org/0000-0002-9016-2438>
 Ranjan Mittal  <https://orcid.org/0000-0003-3729-9352>

References

- [1] Heremans J 2007 *Springer Handbook of Nanotechnology* vol 345 (Berlin: Springer)
- [2] Dresselhaus M S, Chen G, Tang M Y, Yang R G, Lee H, Wang D Z, Ren Z F, Fleurial J-P and Gogna P 2007 *Adv. Mater.* **19** 1043–53
- [3] Lan Y, Minnich A J, Chen G and Ren Z 2010 *Adv. Funct. Mater.* **20** 357–76
- [4] He J and Tritt T M 2010 *Thermal-Electrical Energy Conversion from the Nanotechnology Perspective* (Weinheim: Wiley) pp 47–77
- [5] Yang J and Caillat T 2006 *MRS Bull.* **31** 224–9
- [6] Pei Y, LaLonde A, Iwanaga S and Snyder G J 2011 *Energy Environ. Sci.* **4** 2085–9
- [7] Poudel B et al 2008 *Science* **320** 634–8
- [8] Zhao L-D, Lo S-H, Zhang Y, Sun H, Tan G, Uher C, Wolverton C, Dravid V P and Kanatzidis M G 2014 *Nature* **508** 373–7
- [9] Tang Y, Hanus R, Chen S W and Snyder G J 2015 *Nat. Commun.* **6** 584
- [10] Qiu P F, Yang J, Liu R H, Shi X, Huang X Y, Snyder G J, Zhang W and Chen L D 2011 *J. Appl. Phys.* **109** 063713
- [11] Toberer E S, Brown S R, Ikeda T, Kauzlarich S M and Jeffrey Snyder G 2008 *Appl. Phys. Lett.* **93** 062110
- [12] Tang Y, Gibbs Z M, Agapito L A, Li G, Kim H-S, Nardelli M B, Curtarolo S and Snyder G J 2015 *Nat. Mater.* **14** 1223–8
- [13] Toberer E S, Rauwel P, Gariel S, Taftø J and Jeffrey Snyder G 2010 *J. Mater. Chem.* **20** 9877–85
- [14] Zhang J, Song L, Pedersen S H, Yin H, Hung L T and Iversen B B 2017 *Nat. Commun.* **8** 13901
- [15] Yin H, Christensen M, Pedersen B L, Nishibori E, Aoyagi S and Iversen B B 2010 *J. Electron. Mater.* **39** 1957–9
- [16] Dong H, Li X, Huang X, Zhou Y, Jiang W and Chen L 2014 *Ceram. Int.* **40** 3827
- [17] Zhao D, Tian C, Tang S, Liu Y and Chen L 2010 *J. Alloys Compd.* **504** 552–8
- [18] Walia S et al 2013 *Prog. Mater. Sci.* **58** 1443–89
- [19] Jeong Y K and Choi G M 1996 *J. Phys. Chem. Solids* **57** 81–4
- [20] Hartung D, Gather F, Hering P, Kandzia C, Reppin D, Polity A, Meyer B K and Klar P J 2015 *Appl. Phys. Lett.* **106** 253901
- [21] Young A P and Schwartz C M 1969 *J. Phys. Chem. Solids* **30** 249–52
- [22] Losert W and Hoppe R 1985 *Z. Anorg. Allg. Chem.* **524** 7–16
- [23] Fischer D, Carl W, Glaum H and Hoppe R 1990 *Z. Anorg. Allg. Chem.* **585** 75–81
- [24] Umamaheswari R, Yogeswari M and Kalpana G 2013 *Solid State Commun.* **155** 62–8
- [25] Kresse G and Hafner J 1993 *Phys. Rev. B* **47** 558–61
- [26] Kresse G and Furthmüller J 1996 *Comput. Mater. Sci.* **6** 15–50
- [27] Kresse G and Furthmüller J 1996 *Phys. Rev. B* **54** 11169–86
- [28] Perdew J P, Burke K and Ernzerhof M 1996 *Phys. Rev. Lett.* **77** 3865–8
- [29] Calais J L 1993 *Int. J. Quantum Chem.* **47** 101
- [30] Perdew J P, Ruzsinszky A, Csonka G I, Vydrov O A, Scuseria G E, Constantin L A, Zhou X and Burke K 2008 *Phys. Rev. Lett.* **100** 136406
- [31] Blöchl P E, Jepsen O and Andersen O K 1994 *Phys. Rev. B* **49** 16223–33
- [32] Togo A, Oba F and Tanaka I 2008 *Phys. Rev. B* **78** 134106
- [33] Togo A, Chaput L and Tanaka I 2015 *Phys. Rev. B* **91** 094306
- [34] Ganose A M, Park J, Faghaninia A, Woods-Robinson R, Persson K A and Jain A 2021 *Nat. Commun.* **12** 2222
- [35] Xiao Y et al 2016 *Phys. Rev. B* **94** 125203
- [36] Chang H C, Chen T H, Sankar R, Yang Y J, Chen L C and Chen K H 2020 *Mater. Today Phys.* **15** 100248
- [37] Fujita K, Mochida T and Nakamura K 2001 *Japan. J. Appl. Phys.* **40** 4644–7
- [38] Miller S A, Gorai P, Aydemir U, Mason T O, Stevanović V, Toberer E S and Snyder G J 2017 *J. Mater. Chem. C* **5** 8854–61